phys. stat. sol. (b) **241**, No. 10, 2246–2252 (2004) / **DOI** 10.1002/pssb.200404945

Valence and conduction band offsets of a ZrO_2/SiO_xN_y/n-Si CMOS gate stack: A combined photoemission and inverse photoemission study

S. Sayan[*, 1, 2], R. A. Bartynski[3], X. Zhao[3], E. P. Gusev[4], D. Vanderbilt[3], M. Croft[3], M. Banaszak Holl[5], and E. Garfunkel[, 1]**

[1] Department of Chemistry, Rutgers University, Piscataway, NJ 08854, USA
[2] Semiconductor Electronics Division, National Institute of Standards and Technology, Gaithersburg, MD 20899, USA
[3] Department of Physics and Astronomy, Rutgers University, Piscataway, NJ 08854, USA
[4] IBM T. J. Watson Research Center, Yorktown Heights, New York, USA
[5] Department of Chemistry, University of Michigan, Ann Arbor, MI 48109, USA

Received 15 June 2004, revised 24 June 2004, accepted 1 July 2004
Published online 28 July 2004

PACS 71.20.Ps, 73.20.At, 79.20.Kz, 79.60.Jv

The densities of states above and below the Fermi energy for the ZrO_2/SiO_xN_y/n-Si system are examined by photoemission and inverse photoemission and compared with results from first principles calculations. The measured band gap of ZrO_2 is 5.68 eV and the valence and conduction band offsets relative to silicon are 3.40 and 1.16 eV respectively.

1 Introduction

Silicon dioxide and oxynitrides (SiO_xN_y) are used as the gate dielectrics for MOSFET and related devices because of their excellent insulator properties, low interface trap and bulk defect densities, and their thermal stability. Unfortunately, the ultimate scaling limits for SiO_2 are rapidly approaching due primarily to gate leakage. This leakage current increases the standby power consumption, which is unacceptable especially for low-power applications. Continued scaling requires a <1 nm gate oxide thickness in some applications [1–3].

Instead of thinning the dielectric to obtain the necessary gate stack capacitance, an alternative is to switch to an insulating material with a higher dielectric constant than SiO_2. A physically thicker higher-permittivity layer can be used to maintain low leakage current levels while attaining the necessary capacitance. A large number of alternative gate dielectric materials have been examined during the past few years including metal oxides such as Ta_2O_5, TiO_2, HfO_2, ZrO_2, Y_2O_3, Al_2O_3, and La_2O_3, as well as their silicates and aluminates. Considerable attention has been given to ZrO_2 and HfO_2 due to their relatively high resistivity and dielectric constant ~24.

Selecting a gate dielectric with a higher permittivity than SiO_2 is clearly desirable. Unfortunately, the band gaps of these alternative materials generally decrease as the dielectric constant increases. How these band gaps translate into valence and conduction band offsets next to silicon is also of concern, since the leakage current strongly depends on the band alignment. To first order the gate leakage current

[*] Corresponding author: e-mail: sayan@rutchem.rutgers.edu
[**] e-mail: garf@rutchem.rutgers.edu

density is due to quantum mechanical tunneling and is an exponential function of both the thickness and the barrier height [4, 5]. In general, it increases exponentially with decreasing barrier height and thickness for direct tunneling processes. For electrons tunneling from the substrate silicon into the gate electrode, this is the conduction band offset, and for electrons traveling from the gate to the silicon substrate, this is the barrier height, ϕ_{Bn}. In short, the required need of high permittivity (and capacitance) must be balanced against the decrease in barrier height for tunneling [6] as well as other issues that arise when moving away from SiO_xN_y.

The experimental data on band offsets of alternative dielectric materials with respect to silicon remain limited [7, 8]. On the "theory side", Robertson has performed calculations to determine band offset values for a number of candidate high dielectric materials and this remains one of the more important works in the field [9–11].

Photoemission is probably one of the more reliable techniques to determine valence band offsets. Recently, the number of reports on valence band alignments of alternative gate dielectric materials using XPS has increased. Keister and coworkers studied band offsets for ultrathin SiO_2 and Si_3N_4 films on Si(111) and Si(100) using soft X-ray photoemission spectroscopy [12]. They have found that their spectrum in the valence band edge region was well modeled by a pair of Gaussian-broadened Fermi functions. They obtained band offsets of 4.54 ± 0.1 eV for SiO_2/Si(100) with film thicknesses in the range of 8–12 Å. Hattori studied the SiO_2/Si system with different thicknesses (5–15 Å) regimes using high resolution XPS [13]. Both thickness and angle-resolved analytical procedures were used for analysis of the valence band spectra. Both methods served to eliminate the contributions to the valence band from the silicon in different thickness regimes. During the analysis, it was assumed that the density of states near the valence band edge follows a parabolic energy dependence. It was reported that the top of the valence band of the oxide surface increased by about 0.2 eV near a thickness of 9 Å and was attributed to oxidation-induced stress in the interfacial transition layer. Miyazaki et al. studied Ta_2O_5/Si, ZrO_2/Si and SiO_2/Si high-*k* gate dielectric/silicon interfaces by high resolution XPS and electron energy loss spectroscopy. The energy band gaps were defined as the intercept of a linear extrapolation of the leading edge to the background [8, 14, 15]. Kraut et al. presented XPS results on the determination of core-level to valence-band maximum binding energy differences in GaAs(110), Ge(110) and Ge(111) [16, 17]. They developed a method for determining of the valence band maximum by modeling the XPS valence band spectrum in the vicinity of its maximum by an instrumentally-broadened theoretical valence band density of states and fit the model to experimental data by a least-squares method.

Inverse photoemission (IPE) is a surface spectroscopy complementary to photoemission, which probes the unoccupied electronic states above the Fermi level [18–21]. Unoccupied electronic states are important in helping to understand many diverse material properties such as ferromagnetism and chemisorption, and in the present case, electron conduction in semiconductors. To obtain inverse photoemission spectra, an electron of a well defined energy is directed at a sample and photons are emitted and detected (essentially the opposite of normal photoemission). IPE spectra can be obtained in two different modes: in the isochromat mode the data are obtained by sweeping the kinetic energy of incoming electrons and measuring the intensity of photons at a fixed energy in an inverse photoemission spectrometer. In the fluorescence mode, fixed energy electrons irradiate the surface and the resulting photon spectrum is measured as a function of energy (and in some cases angle). The advantage of the latter is the increased resolution and simultaneous detection of photons over a large range of photon energies.

Ortega et al. studied Si(100), Ge(100) and GaAs(100), mapped the bulk conduction bands by IPE and obtained the critical points with respect to the valence band maximum [22]. Himpsel et al. demonstrated the application of this technique to the study of the SiO_2, Si, and GaAs systems to understand the energy band dispersions for bulk, surface and adsorbate states above the Fermi level which were not accessible by other techniques [23]. They reported that the conduction band density of states for a ~25 Å SiO_2 film on silicon rose continuously until it reached a plateau at about 4 eV above the conduction band minimum. However, it was also reported that the same plateau was reached at around 3 eV for very thin SiO_2 films.

In this paper we present results of PES and IPE for the ZrO_2/SiO_xN_y/Si system. To our knowledge, these represent the first reported inverse photoemission measurements of the ZrO_2 system.

2 Experimental and methods

The ZrO_2 films were grown by atomic layer deposition (ALD) at 300 °C using alternating cycles of $ZrCl_4$ and H_2O; details can be found elsewhere [24]. The substrate used was n-type Si(100) with a doping concentration of ~1×10^{16} cm^{-3}. The thickness of the SiO_xN_y interface film was 8 Å as measured by medium energy ion scattering (MEIS). The soft X-ray measurements were performed at Brookhaven National Laboratories on the U8B beamline using 120–400 eV photon energies. The inverse photoemission studies are done in fluorescence mode in the 20–24 eV electron energy range at Rutgers University. Special attention is given to monitor charging in both photoemission and inverse photoemission. On these samples, charging (as monitored by flux and time dependence) did not cause any spectral changes within experimental error (on thicker samples, charging eventually becomes more prominent).

3 Theory

The amorphous ZrO_2 (a-ZrO_2) models are realized through "melt-and-quench" *ab-initio* molecular-dynamics (MD) simulations [25]. This approach, first pioneered by Car and Parrinello, combines density-functional theory (DFT) with MD into a powerful tool for investigating the physics of large systems, especially for liquids and amorphous structures where the atomic coordinates cannot be obtained from diffraction experiments [26].

We perform *ab-initio* constant-temperature MD as implemented in the VASP simulation package [27], in which the electronic structure is described within DFT [28, 29], in the local-density approximation (LDA) [30], using a plane-wave basis and ultrasoft pseudopotentials [31]. Since VASP currently supports only constant-volume MD simulations, i.e., the volume of a unit cell is fixed during a "melt-and-quench" simulation, we thus carry out a series of similar MD simulations on several candidate supercells of different volumes to study the influence of volume on the resultant structure [25]. The a-ZrO_2 is modeled to have periodic boundary conditions with a cubic supercell containing 96 atoms. This is the same content as a $2 \times 2 \times 2$ repetition of the monoclinic unit cell. We have reduced the plane-wave cutoff energy to 15 Ry, and the pseudopotential for Zr includes only the outermost shells (4d, 5s) in the valence. It is found that the chosen pseudopotentials and plane-wave cut-off are adequate to correctly reproduce the structures and energetics of the three ZrO_2 phases (cubic, tetragonal, and monoclinic). Given the supercell size of $2 \times 2 \times 2$, our MD simulations are done using single *k*-point sampling at the Γ point of the Brillouin zone. One candidate cell, fortunately, leads successfully to a reasonable amorphous model of ZrO_2 [25]. The density of states (DOS) function is calculated on this generated model using VASP. We used a refined mesh of *k*-points ($2 \times 2 \times 2$) and higher 30-Ry cut-off energy to obtain a smoother and more accurate DOS function. While the valence DOS is computed by summing over all 256 occupied bands, the conduction DOS is obtained from just the first 160 unoccupied bands, leading to an artificial cutoff of the DOS, visible in Fig. 3, at around 7.8 eV.

4 Results and discussion

Figure 1 presents the Zr 3d and 4p regions of the soft X-ray photoemission spectra obtained at 160 and 240 eV photon energies of 30 Å ZrO_2/SiO_2/n-Si(100) respectively. Curve fitting was performed after a Shirley background subtraction. A pair of Gaussians is used to model these regions representing the spin–orbit splittings of the 3d and 4p levels. The spin–orbit splittings were found be 2.38 and 1.57 eV for the 3d and 4p levels respectively. The intensity ratios were ~3 : 2 and ~2 : 1, in agreement with the expected theoretical ratio. The binding energies of the $3d_{5/2}$ and $4p_{1/2}$ peaks are 183.78 and 31.82 eV, respectively.

The photoemission and inverse photoemission data obtained from a 30 Å ZrO_2/SiO_xN_y/n-Si are shown in Fig. 2. The valence band mainly consists of O 2p-like non-bonding orbitals of π-symmetry while the conduction band is mainly Zr 5d-like anti-bonding orbitals. The energy separation between the Fermi level and the valence band maximum (VBM) and conduction band minimum (CBM) are found to be 4.32 and 1.36 eV, respectively. Hence the band gap is extracted to be 5.68 eV. As a note of caution, we mention that semiconductor energy gaps are specific to the method(s) used to determine them. It is also

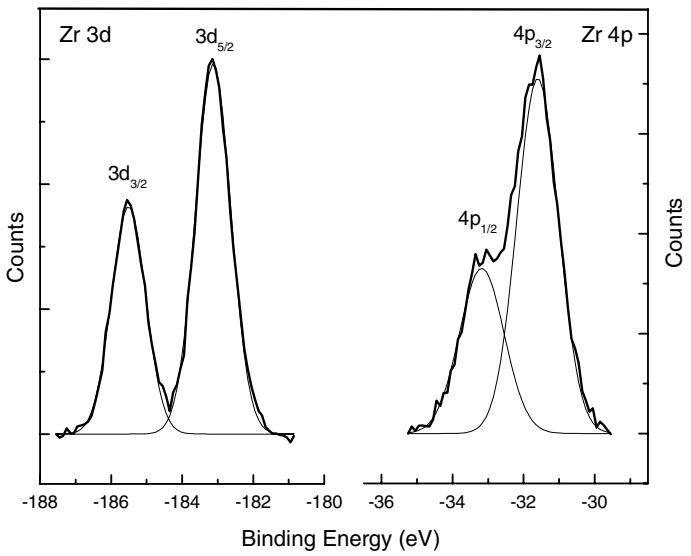

Fig. 1 Zr 3d and 4p regions of ZrO_2/SiO_xN_y/n-Si sample.

important to note that photoemission and inverse photoemission give a one particle energy gap that, although wider than the conventionally reported optical gap (which usually involves an exciton), may be more relevant to understanding tunneling through a dielectric. Other methods of gap and edge determination such as spectroscopic ellipsometry (SE), UV/VIS spectroscopy, XPS shake up spectral analysis, near-edge XAS, include the exciton gap which may be as high as 1–2 eV in some oxides.

All energies are referenced to the Fermi level which is determined by a clean polycrystalline gold foil. Special care is taken when determining the spectrometer response functions for both IPE and PES. This is carefully accomplished by modeling the region in the vicinity of the Fermi level by a step function and a Gaussian function whose width is found to represent the spectrometer response function. The thermal broadening is negligible in comparison to the spectrometer broadening. In the case of photoemission experiments, the obtained spectrometer response is cross-checked with the width of the Au 4f doublet which is equal to the combined broadening due to core-hole lifetime and spectrometer response. In this case, the core-hole lifetime for Au $4f_{7/2}$ is calculated to be 0.32 eV in accordance with literature values

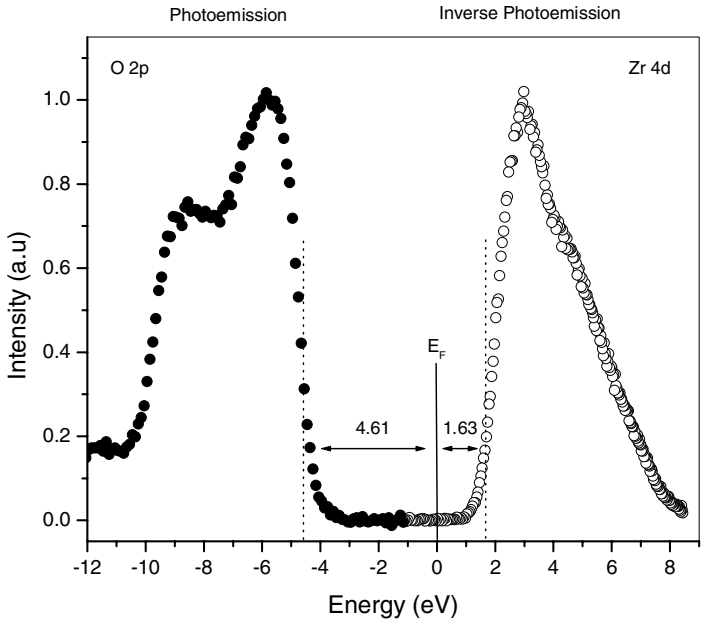

Fig. 2 Combined photoemission (full circles) and inverse photoemission (open circles) spectra of a 30 Å ZrO_2/SiO_xN_y/ n-Si gate stack.

[17, 32]. The spectrometer response functions had Gaussian widths of 0.67 and 0.50 eV for photoemission and inverse photoemission experiments respectively.

As the crystal structure of this particular sample was previously determined by XAS and XRD to be amorphous, only the theoretical density of states for amorphous ZrO_2 is considered [33]. Although the band gap is not calculated exactly in this method, the shapes and densities of state of occupied and unoccupied band are thought to be accurate. In order to determine the VBM and CBM position, we have employed the following procedure, analogous to the procedure employed by Kraut et al. [17]. First the theoretical density of states for amorphous ZrO_2 is convoluted with the appropriate spectrometer response functions for both PES and IPES spectra. The height of the first peak below (above) the VBM (CBM) is normalized to unity. Then the broadened theoretical curves in the band edge region are shifted until they align with the experimental curves (Fig. 3). The VBM and CBM are determined from the band structure calculation, and yield an energy gap of 2.81 eV. Then the corresponding energy shifts needed to align the experimental and theoretical densities of states are added to this theoretical gap to obtain the experimental band gap which is found to be 5.68 eV. If on the other hand, we take the conventional method of linear extrapolation of the valence and/or conduction band leading edge to the background intensity level, we obtain a value of 5.66 eV for the band gap and 3.29 and 1.27 for valence and conduction band offsets respectively. In this case, the straight line method yields a very similar result.

Figure 3a shows the theoretical density of states of valence and conduction bands respectively. In Fig. 3b, the theoretical density of states is convoluted with the instrumental response function, and is plotted along with the experimental measurement of valence and conduction bands. Good agreement is observed between the experimental and theoretical valence band density of states (specifically the band widths and edges), even though the theoretical density of states is not modified for photoemission cross-sections (transition matrix elements). However one would expect that the scattering cross-section across the band would be similar (if not the same) since the valence band is almost exclusively made up of oxygen 2p-like orbitals of σ- and π-symmetries. In the case of the unoccupied conduction band, the width of the band and the band edge structures agree well with theory, although the intensity in the upper portion of the band is not in agreement. This discrepancy may result from differences in cross-sections. This is somewhat expected since the atomic d-orbitals split due to the crystal field, and they do have different symmetries. To a first approximation, assuming a cubic field around zirconium cations, the orbitals should split into doubly degenerate e_g and triply degenerate t_{2g}-orbitals. It should also be noted that the theoretical calculations are based on the ground state of the system; on the other hand, the measurement is inherently representative of excited states. We also note that our recent X-ray absorption studies on the L_2 and L_3 edges of ZrO_2 showed significant matrix element effects, which indicates different cross-sections for these orbitals [33].

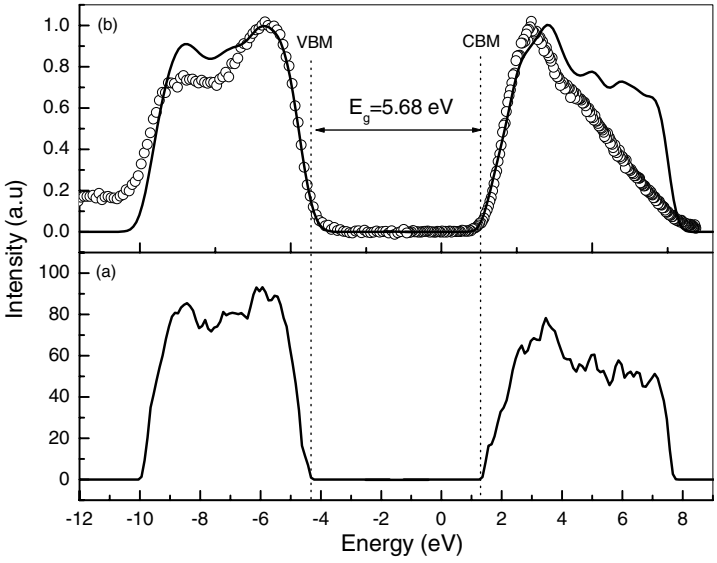

Fig. 3 (a) Theoretical density of states (DOS) for amorphous ZrO_2. Valence band (left) and conduction band (right) have each been independently shifted for best alignment. (b) Solid curve: theoretical DOS of panel (a), broadened by experimental response functions. Symbols: experimental photoemission (left) and inverse photoemission (right) spectra of ZrO_2 thin films.

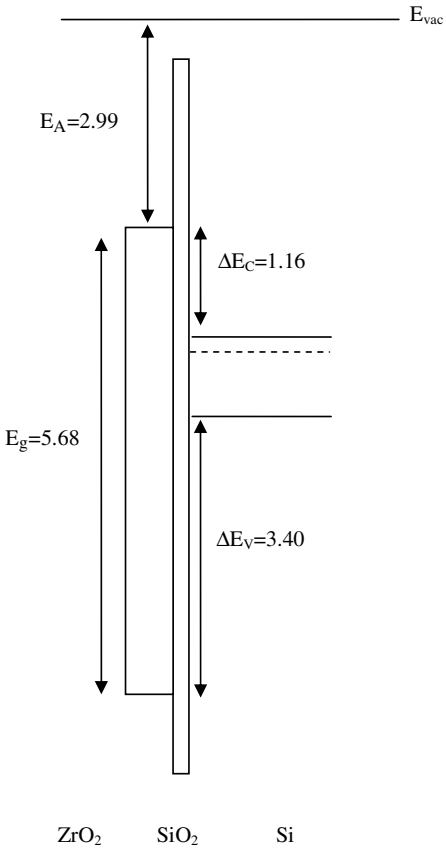

Fig. 4 Simplified energy band diagram of ZrO_2/SiO_xN_y/n-Si gate stack.

In order to extract the valence and conduction band offsets, a knowledge of the Fermi level within the silicon bandgap is required. The substrate used is an n-type Si with a doping concentration of 1×10^{16} cm^{-3}. The position of the Fermi level with respect to the CBM and VBM can be calculated accordingly. To obtain the offsets, the energy separation between the Fermi level and CBM is subtracted from the position of the CBM with the respect to the Fermi level. Figure 4 shows a simplified energy band diagram for this gate stack. The obtained valence and conduction band offsets (3.40 and 1.16 eV) are large enough to make ZrO_2 a viable candidate from a band alignment point of view. These values are in good agreement with the ones reported by Robertson [9]. However in order to be able to compare the values obtained, one would need to know the phase of the ZrO_2 reported in these studies. Having known the electron affinity of silicon and the conduction band offset, the electron affinity of ZrO_2 can be extracted as 2.99 eV. This is the first experimental value reported to date to the best of our knowledge. Our current studies are aimed to determine the effect of electric field and potential across the gate stack since these effects will be operative in band alignment.

Another important outcome of this study is that the energy separation between the Zr $3d_{5/2}$, Zr $4p_{3/2}$ and VBM are determined. The energy separation between a given core level and the VBM is constant for given material. This way, by measuring the binding energy of these core levels, one can easily locate the VBM for a given ZrO_2 system. The energy separation between ΔE (Zr $3d_{5/2}$–VBM) and ΔE (Zr $4p_{3/2}$–VBM) are 179.17 and 27.21 eV respectively.

5 Conclusion

The valence and conduction band offsets of the ZrO_2/SiO_xN_y/n-Si gate stack structure are determined by comparing photoemission and inverse photoemission results with theoretical calculations of the occupied

and unoccupied densities of states. The measured band gap is 5.68 eV and the valence and conduction band offsets with respect to silicon are 3.40 and 1.16 eV, respectively. The electron affinity of ZrO_2 is found to be 2.99 eV.

Acknowledgements We thank the Semiconductor Research Corporation and Sematech International for financial support. S. Sayan and E. Garfunkel would like to thank J. Robertson, R. Opila and S. Chambers for useful discussions, and A. Danese and R. Bersch for technical support. David Vanderbilt acknowledges NSF Grant DMR-0233925 for financial support.

References

[1] ITRS (International Technology Roadmap for Semiconductors, 2003).
[2] E. P. Gusev, E. Cartier, D. A. Buchanan, M. Gribelyuk, M. Copel, H. Okorn-Schmidt, and C. D'Emic, Microelectron. Eng. **59**, 341–349 (2001).
[3] M. L. Green, E. P. Gusev, R. Degrave, and E. Garfunkel, J. Appl. Phys. **90**, 2057–2121 (2001).
[4] E. H. Nicollian and J. R. Brews, MOS Physics and Technology (John Wiley & Sons, New York, 1982).
[5] S. M. Sze, Physics of Semiconductor Devices, second ed. (John Wiley & Sons, New York, 1981).
[6] G. D. Wilk, R. M. Wallace, and J. M. Anthony, J. Appl. Phys. **89**, 5243 (2001).
[7] V. V. Afanas'ev, A. Stesmans, F. Chen, X. Shi, and S. A. Campbell, Appl. Phys. Lett. **81**, 1053–1055 (2002).
[8] S. Miyazaki, Appl. Surf. Sci. **190**, 66–74 (2002).
[9] J. Robertson, J. Vac. Sci. Technol. B **18**, 1785–1791 (2000).
[10] L. R. C. Fonseca, A. A. Demkov, and A. Knizhnik, phys. stat. sol. (b) **239**, 48–58 (2003).
[11] R. Puthenkovilakam, E. A. Carter, and J. P. Chang, Phys. Rev. B **69**, 155329 (2004).
[12] J. W. Keister, J. E. Rowe, J. J. Kolodziej, H. Niimi, T. E. Madey, and G. Lucovsky, J. Vac. Sci. Technol. B **17**, 1831–1835 (1999).
[13] T. Hattori, in: Fundamental Aspects of Ultrathin Dielectrics on Si-based Devices, Proc. of NATO Advanced Research Workshop, St. Petersburg, Russia, August 1997, edited by E. Garfunkel, E. Gusev, and A. Vul' (Kluwer Academic Publishers, Dordrecht, 1997), p. 241–256.
[14] S. Miyazaki, J. Vac. Sci. Technol. B **19**, 2212–2216 (2001).
[15] S. Miyazaki, M. Narasaki, M. Ogasawara, and M. Hirose, Solid-State Electron. **46**, 1679–1685 (2002).
[16] E. A. Kraut, R. W. Grant, J. R. Waldrop, and S. P. Kowalczyk, Phys. Rev. Lett. **44**, 1620–1623 (1980).
[17] E. A. Kraut, R. W. Grant, J. R. Waldrop, and S. P. Kowalczyk, Phys. Rev. B **28**, 1965–1977 (1983).
[18] V. Dose, Prog. Surf. Sci. **13**, 225–283 (1983).
[19] V. Dose, Appl. Phys. **14**, 117–118 (1977).
[20] F. J. Himpsel, T. Fauster, and D. Straub, J. Lumin. **31–32**, 920–926 (1984).
[21] N. V. Smith, Vacuum **33**, 803–811 (1983).
[22] J. E. Ortega and F. J. Himpsel, Phys. Rev. B **47**, 2130–2137 (1993).
[23] F. J. Himpsel and D. Straub, Surf. Sci. **168**, 764–772 (1986).
[24] M. A. Gribelyuk, A. Callegari, E. P. Gusev, M. Copel, and D. A. Buchanan, J. Appl. Phys. **92**, 1232–1237 (2002).
[25] X. Zhao and D. Vanderbilt, Phys. Rev. B (2004), submitted.
[26] R. Car and M. Parrinello, Phys. Rev. Lett. **55**, 2471–2474 (1985).
[27] G. Kresse and J. Hafner, Phys. Rev. B **47**, 558–561 (1993).
[28] P. Hohenberg and W. Kohn, Phys. Rev. B **136**, 864–871 (1964).
[29] W. Kohn and L. J. Sham, Phys. Rev. A **140**, 1133–1138 (1965).
[30] D. M. Ceperley and B. J. Alder, Phys. Rev. Lett. **45**, 566–569 (1980).
[31] D. Vanderbilt, Phys. Rev. B **41**, 7892–7895 (1990).
[32] P. H. Citrin and G. K. Wertheim, Phys. Rev. Lett. **41**, 1425–1428 (1978).
[33] S. Sayan, T. Emge, E. Garfunkel, M. Croft, X. Zhao, D. Vanderbilt, N. V. Nguyen, J. Ehrstein, I. Levin, E. P. Gusev, H. Kim, and P. J. McIntyre, Appl. Phys. Lett. (2004), submitted.